J. Biochem. 132, 863–874 (2002)

pH-Dependent Aggregate Forms and Conformation of Alzheimer Amyloid β-Peptide (12–24)

Hiroshi Abe,*,† Kazunori Kawasaki,‡ and Hiroshi Nakanishi*,†,1

Biological Information Research Center, National Institute of Advanced Industrial Science and Technology, 1-1 Higashi, Tsukuba, Ibaraki 305-8566; †Department of Biological Science and Technology, Science University of Tokyo, 2641 Yamazaki, Noda, Chiba 278-0022; and ‡Institute of Molecular and Cell Biology, National Institute of Advanced Industrial Science and Technology, 1-1 Higashi, Tsukuba, Ibaraki 305-8566

Received July 5, 2002; accepted August 26, 2002

The conformational transition to a β-structure and the aggregation process of Alzheimer amyloid β-peptide (12–24) [abbreviated as $A\beta_{12-24}$] were studied. The influence of sample dissolution methods for the aggregate structure was examined by electron microscopy (EM). The difference in the width of the aggregate of $A\beta_{12-24}$ depended on the pH immediately after sample dissolution. Two types of sample dissolution methods, F and R, were employed. For dissolution method F, the peptide sample was immediately dissolved in water and then adjusted to pH 2.2 by adding buffer, while for dissolution method R, the peptide was directly dissolved in the buffer solution. In the latter case, the starting pH was 3.0. Slight fibrils (10–12 nm in diameter) were observed with method F, and wider ribbon-like aggregates (17–20 nm in diameter) with method R, despite the same pH range. A difference between methods F and R was also detected in the CD spectra, especially at pHs near 5.0. The CD intensity of the 214 nm band with method R changed with pH, with the highest value at pH 3.7, whereas that with method F was unchanged at pHs below 5.0. The temperature-dependent CD results showed that a thermostable aggregate of $A\beta_{12-24}$ occurs at higher pHs than 3.0. NMR analysis showed that deprotonation of the C-terminal carboxylate group in $A\beta_{12-24}$ triggered the aggregate formation, and the transition from a random coil to a β-conformation in the C-terminal region of V18–V24 was detected on analysis of the $^3J_{\alpha N}$ coupling constant in the pH range of 2.2 to 3.0.

Key words: aggregate form, amyloid beta-peptide, circular dichroism, electron microscopy, NMR.

Senile plaques associated with Alzheimer's disease contain insoluble deposits of fibrils formed by the 39–43 amino acid peptide of amyloid-β (Aβ) with possible neurotoxic effects (*1*). Aβ is known to secrete from amyloid precursor protein in soluble form (*2*), and the structural conversion to a supramolecular aggregate is attributed to neurotoxic activity (*3, 4*).

Structural studies on Aβ have provided insights into the organization of Aβ assemblies and the kinetics of Aβ polymerization (*5*). From a pathological point of view, the study of a full-length peptide (such as $A\beta_{1-40}$ and $A\beta_{1-42}$) is most appropriate. However, a structural study of a full-length peptide by means of high-resolution structural techniques involves difficulties such as signal broadening, overlapping, and poor solubility for NMR analysis, and noncrystallinity for X-ray crystallography. On the other hand, from the point of view of structural biology, the study of an Aβ fragment peptide is important due to the ability of polymerization, fibrillation, and inhibition of Aβ-fibrillogenesis (*6–9*). Studies on a fragment peptide capable of forming fibrils have contributed to the structural analysis of not only Aβ (*10–15*) but also other conformational-disease related proteins (*16–18*).

In the amino acid sequence of Aβ, the region from K16 to A21 ($A\beta_{16-21}$) is known to be important for fibrillogenesis (*19–22*). The region from L17 to A21, called the "hydrophobic core," is essential for fibrillization of full-length β-amyloid peptide (*19*). Pentapeptide $A\beta_{16-20}$ binds to full-length Aβ and prevents its assembly into amyloid fibrils (*20, 21*). Short fragment peptides of Aβ such as pentapeptide $A\beta_{16-20}$ do not form fibrils, existing monomerically (*22*).

Tjernberg *et al.* reported regarding short fragment peptides of Aβ that undecapeptide $A\beta_{13-23}$ and all fragment peptides longer than 11 residues formed fibrils similar to full-length Aβ (*23*). Recently, Balbach *et al.* reported that among Aβ fragment peptides containing the central hydrophobic core, the shortest peptide forming fibrils is heptapeptide $A\beta_{16-22}$ (*24*).

Several kinds of amyloid peptide assemblies during fibrillogenesis have been reported for Aβ and its fragment peptides (*5, 8, 9, 25–30*). A fibril structure was generally

The nomenclature for the atoms of amino acids as to NMR signals conform to the recommendations of Markley *et al.* (*70*).

[1]To whom correspondence should be addressed. Tel: +81-298-61-6136, Fax: +81-298-61-6135, E-mail: hiroshi-nakanishi@aist.go.jp

Abbreviations: 1D, 2D, one- and two-dimensional; Aβ, amyloid β-peptide; C-terminal, carboxyl terminal; COSY, correlation spectroscopy; E-COSY, exclusive correlated spectroscopy; EM, electron microscopy; HMQC, heteronuclear multiple quantum coherence; N-terminal, amino-terminal; NOE, nuclear Overhauser enhancement; NOESY, nuclear Overhauser effect spectroscopy; TOCSY, total correlation spectroscopy.

observed among these Aβ assemblies, which exist as a mixture of straight and twisted fibers (*27*), while for some short fragment peptides of Aβ of less than 20 amino acid residues, a ribbon-like aggregate was reported (*8, 9*). Electron microscopy (EM) has shown that ribbon-like aggregates are wider and thinner than fibrils. Recent studies on Aβ revealed that the protofibrils and soluble oligomers exhibit higher neurotoxicity than matured fibrils (*4, 28*). To understand how the different kinds of aggregates are formed, we must clarify the association mechanism of Aβ molecules, which is accompanied by secondary structural conversion from an α-helical or random-coil structure into a β-conformation (*7, 13, 31*).

For the present study, we chose fragment peptide $A\beta_{12-24}$, $VHHQ_{15}KLVFF_{20}AEDV$, as a useful model of Aβ to study the conformational transition and polymorphism of a peptide aggregate. $A\beta_{12-24}$ is highly water-soluble and NMR detectable under acidic pH conditions, in spite of the fact that the β-conformational feature was observed on circular dichroism spectroscopy (CD). Interestingly, two types of aggregate, *e.g.* ribbons and fibrils, were found with different sample preparation methods, R and F, despite the same pH. The secondary structure and dynamic behavior of the peptide in a solution were studied by means of CD and high-resolution NMR spectroscopy. The influence of pH on the conformation and aggregate forms of $A\beta_{12-24}$ is discussed.

METHODS

Peptide Synthesis—$A\beta_{12-24}$ was synthesized by means of the Fmoc strategy using a simultaneous multiple peptide synthesizer, Model PSSM-8 (Shimadzu, Kyoto). Each residue was coupled for 30 min with PyBOP/HOBt (Watanabe Chemical Industries, Hiroshima). The peptide was cleaved from the Alko-resin (Watanabe Chemical Industries) using 5% anisole and 1% 1,2-ethanedithiol in trifluoroacetic acid for 1.5 h at room temperature. The cleaved peptide was washed with diethyl ether and then solubilized with 25% acetonitrile in 0.01 N HCl.

Crude $A\beta_{12-24}$ was purified by reverse phase HPLC on an ODS column (20 mm × 150 mm) heated at 40°C with a linear gradient of 25 to 35% acetonitrile in an aqueous solution of 0.01 N HCl over 10 min at a flow rate of 9.9 ml/min. The molecular weight of the peptide was determined by matrix-assisted laser desorption/ionization time-of-flight mass spectrometry (MALDI-TOF MS). The peptide purity was greater than 95%, as judged on analytical HPLC. The purified peptides were lyophilized and stored at –20°C until used.

Preparation of Peptide Samples—The samples of the synthetic fragment peptide $A\beta_{12-24}$ used in this study were prepared at a concentration of 2 mM in solvent buffered with 10 mM sodium phosphate, except for the special concentration described in the text.

All pH measurements were performed with a HM-30V pH meter (TOA) with an electrode for 5 mm NMR tubes (GST-5428S; TOA). Standard aqueous buffers were used for electrode calibration at pH 4 and 7.

Sample preparation was performed by two different methods, R and F. The pH immediately after sample dissolution for method R is 3.0, and that for method F is 2.2. A lyophilized sample was used as the starting sample for both preparation methods. A sample solutions for Method R (pH 3.0) were prepared by dissolving $A\beta_{12-24}$ in a 10 mM sodium phosphate buffer solution obtained by diluting of the stock buffer of 100 mM sodium phosphate solution, pH 4.6. The samples were kept on ice for 30 min, and then the pH was adjusted for each experiment with small aliquots of a 50 or 500 mM NaOH solution, or phosphoric acid. The sample solutions for Method F were prepared by directly dissolving $A\beta_{12-24}$ in water, the pH being controlled at 2.2 with phosphoric acid. After the samples had been kept on ice for 30 min, 100 mM phosphate buffer, pH 1.6, was added to 10 mM, and then the pH was adjusted similarly to in the case of method R.

For the concentration-dependent experiments, samples of 31–125 μM were dissolved in water at 2 mM on ice, and then the samples were diluted to each concentration with 100 mM sodium acetate buffer to give a final 10 mM buffer solution (pH 5.0).

Experimental errors of pH within ± 0.1 were neglected for the samples in this study.

For NMR samples, NaOD and D_2O were used instead of NaOH and H_2O. pH measurements for the NMR samples were not corrected for deuterium isotope effects.

Electron Microscopy—To observe the aggregate of $A\beta_{12-24}$ by EM, peptide samples (2 mM) were incubated in 10 mM sodium phosphate buffer for 6 days at 37°C.

A droplet of each sample was put on a 400 mesh copper grid (VECO, The Netherlands) coated with collodion, and then negatively stained with 1% uranylacetate for about 1 min, excess staining solution being removed with filter paper. The specimens were allowed to dry, coated with carbon in a vacuum evaporator (JEE-400; JEOL, Tokyo), and then observed by transmission EM (H-7000; Hitachi, Tokyo), at 75 kV.

Electron micrographs were scanned into a personal computer. The widths of aggregates were measured in 150 points for fibrils at pH 3.7 and for ribbons at pH 3.6, using software GIMP (Peter Mattis and Spencer Kimball).

Circular Dichroism Spectra—CD spectra were recorded with a Jasco J720 spectropolarimeter from 250 to 190 nm, every 0.2 nm with a 2 s integration-time and a 1 nm bandwidth. Four scans were averaged. The path length of the quartz cell was 10, 1, or 0.1 mm, depending on the sample concentration.

All spectra were corrected by subtracting the baseline of the solvent buffer solution recorded under the same conditions. The results are expressed as mean residue ellipticity [θ] in units of degrees cm^2 $dmol^{-1}$.

The temperature was controlled with a refrigerated bath and circulator (HAAKE, DG-8), and read with a resistance thermometer sensor (CHINO DB1000). The temperature was changed within 4–90°C with 2°C intervals every 5 min. For CD spectra at wavelengths of 230–200 nm, three scans were averaged.

NMR Experiments—Peptide samples for NMR measurements were dissolved in H_2O/D_2O 9:1 (v/v) or D_2O with 10 mM sodium phosphate, minute amounts of phosphoric acid being added to adjust the samples to under pH 2.6. Sodium 3-(trimethylsilyl)-propane sulfonate in a capillary tube was used as the standard for NMR chemical shifts.

Standard DQF-COSY (*32, 33*), TOCSY (*34*), and NOESY (*35*) spectra were recorded at both 5°C and 25°C with either a Bruker DMX-500 or DMX-750 spectrometer.

Two-dimensional NMR data were transferred to an Indigo 2 (Silicon Graphics) computer workstation and processed using the nmrPipe/nmrDraw program (36) (Biosym/Molecular Simulations) or XWIN-NMR (Bruker Instruments). Usually, a sine-squared window function shifted by $\pi/4$–$\pi/2$ was applied in both dimensions, with zero filling in f1 to 2K points. Quadrature detection in f1 was achieved with TPPI (*37*). H_2O resonance was suppressed either by presaturation of the solvent peak during the relaxation delay (and the mixing time for the NOESY spectra) or by using a pulsed-field gradient technique with a WATERGATE sequence (*38, 39*). Generally, spectra were collected with 2 K points in f2 and 512 in f1.

E-COSY experiments (*40*) with 512 FIDs in the f1-dimension and 4K points in f2 were zero filled to 2K points in the f1-dimension prior to Fourier transformation. Mixing times of 60 ms were used in TOCSY experiments. Lorentz-to-Gauss filtering functions were applied in the second dimension.

The ^{13}C-^{1}H HMQC experiment at ^{13}C natural abundance

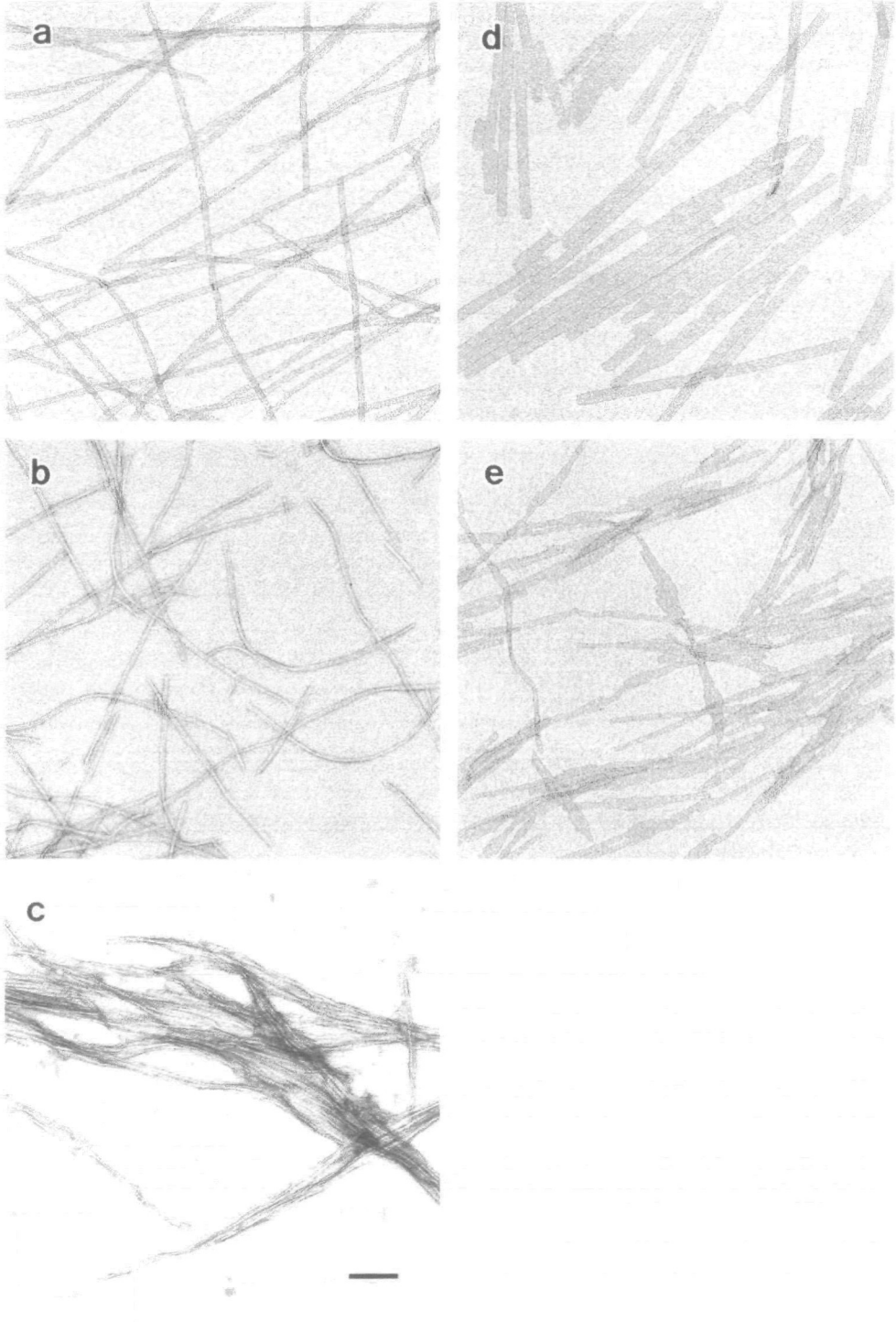

Fig. 1. **Electron micrographs of $A\beta_{12-34}$. All samples were incubated for 6 days at 37°C.** Samples for method F were prepared at pH 3.7 (a), pH 5.1 (b), and pH 6.6 (c). Samples for method R were prepared at pH 3.6 (d), and pH 5.1 (e). The scale bar represents 100 nm. The peptide concentrations were 2 mM except in (c) (640 μM).

was conducted with a D_2O sample of $A\beta_{12-24}$ at a peptide concentration of 2 mM.

Natural abundance ^{13}C heteronuclear HMQC spectra (*41*) were recorded at 5°C with a GARP ^{13}C-decoupling sequence (*42*). 128 scans were acquired for each of 512 t1 values. The spectral width in w2 was 8,000 Hz and that in w1 was 22,497 Hz.

The ^1H and ^{13}C NMR signals of $A\beta_{12-24}$ were assigned using standard sequential assignment procedures (*43*).

pH Titration of ^1H NMR Chemical Shifts of $A\beta_{12-24}$—The dependence of proton chemical shifts of the peptide on the pH of the sample solution was monitored by performing a total of 10 2D TOCSY experiments at pH 2.3–7.7. $A\beta_{12-24}$ was dissolved in 90% H_2O/10% D_2O at a concentration of 250 μM with 10 mM sodium phosphate, and the spectra were recorded at 25°C with a Bruker DMX-750 spectrometer.

The pH of the samples was read before and immediately after the NMR experiments, and the latter measurement was applied to pH titration experiments.

The chemical shifts of E22 H^{γ}, D23 $H^{\beta 1}$, D23 $H^{\beta 2}$, and V24 H^{α} were analyzed to determine each carboxyl pK_a value.

pK_a values were calculated by nonlinear least-squares fitting of experimental pH titration curves to the following equation,

$$\delta = [\delta_{acid} + \delta_{base} 10^{(pH - pK_a)}]/[1 + 10^{(pH - pK_a)}],$$

where δ_{acid} and δ_{base} represent the chemical shifts at low and high pH extremes, respectively. The equation was derived from the Henderson-Hasselbach equation assuming a rapid equilibrium between protonated and unprotonated forms (*44*).

RESULTS

To determine whether or not the sample preparation method for $A\beta_{12-24}$ influences the conformation of the peptide and its aggregate structure, we studied two sample dissolution methods—conventional "method R" and modified "method F"—as follows: A method R sample was first dissolved in a phosphate-buffered solution, resulting in an initial solution pH of *ca.* 3.0, and the pH was changed for different pH experiments. A method F sample was dissolved in water and the pH of the solution was adjusted to 2.2 by adding small aliquots of phosphoric acid (for details see "METHODS"). Two types of aggregates of $A\beta_{12-24}$ due to the two dissolution methods were observed on EM. To obtain molecular conformational information on $A\beta_{12-24}$ and detailed chemical environments at atomic resolution in the solution state, we obtained CD and NMR spectra under different sample conditions.

Electron Microscopy—The morphologies of aggregates of β-amyloid fragment peptide $A\beta_{12-24}$ prepared by the two protocols (dissolution methods F and R) were compared in the same pH range by negative staining electron microscopy (Fig. 1). The distribution patterns of the width of the aggregates in the samples at pH 3.7 with method F and at pH 3.6 with method R are shown in Fig. 2.

An electron micrograph of $A\beta_{12-24}$ at pH 3.7 with method F revealed straight filamentous aggregates (Fig. 1a). Individual filaments obtained with method F at pH 3.7 had a uniform width of *ca.* 10 nm (Fig. 2). At pH 5.1 with method F, however, each fibril seemed to be more flexible and twisted than at pH 3.7, so the width varied from locus to locus even along the same fibril (Fig. 1b). Consequently, narrower fibrils appeared at pH 5.1 than at pH 3.7. These fibrils at pH 3.7 and 5.1 are consistent with previously reported fibrils of full-length Aβ (*45*). There appeared to be no sign of specific interaction between fibrils. At pH 6.6, intensive lateral clustering of fibrils was induced, bundles of fibrils being formed (Fig. 1c). Under these conditions, white granules in the sample solution were observable to the naked eye.

In contrast to the results with method F, ribbon-like assemblies of *ca.* 19 nm in width were observed with method R at pH 3.6 (Figs. 1d and 2), similar to the structure reported by Gorevic *et al.* (*8*) and Fraser *et al.* (*9*). The ribbons were flat and straight on the collodion film, twisted portions being rare (Fig. 1d). Although individual ribbons initially appeared to be almost uniform in width, closer observation showed that the width of several ribbons changed with the position along the ribbons. It can be pointed out that the distribution of the aggregate width with method R is considerably larger than that with method F (Fig. 2). At pH 5.1 with method R (Fig. 1e), the ribbons were clustered and twisted portions were frequent.

In brief, comparison of the aggregate structures derived with the two dissolution methods clearly showed that $A\beta_{12-24}$ assumes different aggregate structures, *i.e.*, fibrils or ribbons, at the same pH.

CD Spectra at Different pHs—To obtain information on the influence of the solution pH and sample dissolution method on the secondary structure, CD spectra of $A\beta_{12-24}$ were measured at different pHs with both methods.

On CD spectral measurement at pH 2.1–3.7 with method R (Fig. 3A), the CD spectrum at pH 2.1 showed a weak positive band near 220 nm, a distinctive feature of random coil, while the CD spectra between pH 3.0 and 3.7 showed a distinct minimum at 214 nm, a characteristic signature of the β-conformation structure. The intensity of this minimum band increased with increasing pH. The spectra at pH 2.1–3.7 showed a well defined isodichroic point at 209 nm, evidence of a simple two-state conformational equilibrium between β-sheet and random coil. Since no accurate established method exists for determining the amounts of

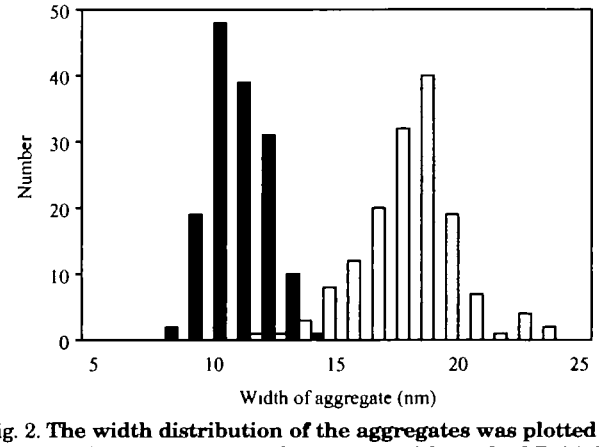

Fig. 2. **The width distribution of the aggregates was plotted at pH 3.7 with method F (■) and at pH 3.6 with method R (□) for 150 points.** Each width was ranked every 1 nm.

β-structure in peptides, we tentatively estimated the population of the β-conformation in $A\beta_{12-24}$ as 0% β-conformation at pH 2.1 and 100% at pH 3.7, resulting in a β-conformation population of 27% at pH 2.7, 65% at pH 3.0, and 83% at pH 3.3 as to the CD intensity of the negative band at 214 nm (θ_{214}). Increasing the pH from 3.7 to neutral caused a decrease in θ_{214} intensity with method R. It did not overlap with the isodichroic point of 209 nm.

Under acidic conditions of less than *ca.* pH 4, CD bands of the β-conformation with both methods R and F showed a similar sharp negative minimum at 214 nm (data not shown). At nearly neutral pH, however, distinct spectral differences were seen between samples with methods R and F at pH 5.2 (Fig. 3B). In the spectrum with method R, another negative minimum band was observed at 226 nm, but no such band was seen in the spectrum with method F despite that the pH was the same. These results clearly indicated a difference in the higher-order structure between the two samples.

At pH 5.5 with method F, the sample solution exhibited high viscosity and, somewhat surprisingly, the negative band shifted near 216 nm (Fig. 3B-c). At a more neutral pH, visible aggregates appeared in the sample solution and the CD spectrum showed very weak absorption at all wavelengths, probably due to generic light scattering (data not shown).

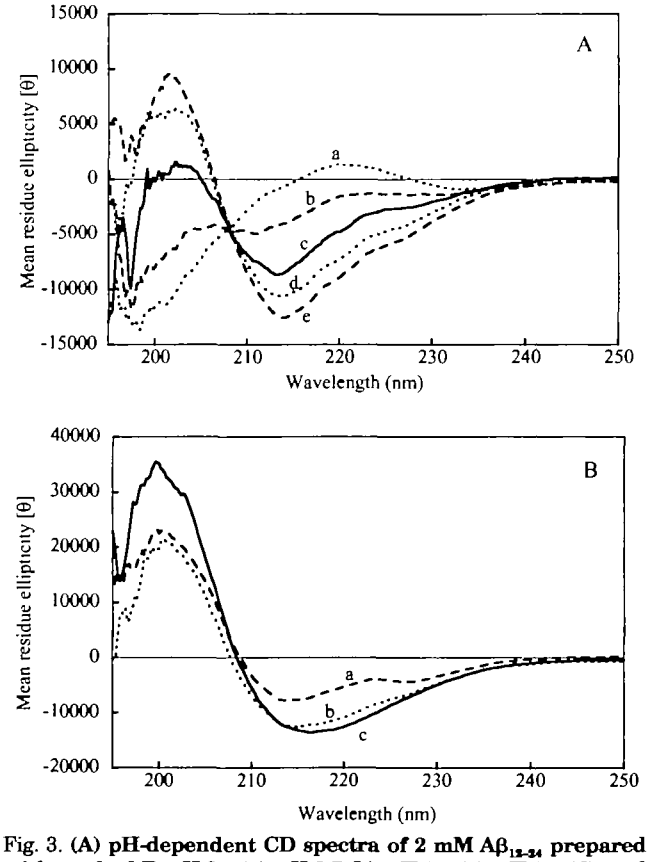

Fig. 3. **(A) pH-dependent CD spectra of 2 mM $A\beta_{12-24}$ prepared with method R: pH 2.1 (a), pH 2.7 (b), pH 3.0 (c), pH 3.3 (d), and pH 3.7 (e). (B) Different CD spectra of 2 mM $A\beta_{12-24}$ prepared with methods R and F.** (a) pH 5.2 with method R, (b) pH 5.2 with method F, and (c) pH 5.5 with method F. All spectra were recorded at 25°C. Mean residue ellipticities ([θ], degrees cm^2 $dmol^{-1}$) were not corrected for the effect of sample aggregation.

Temperature-Dependent CD Spectra of $A\beta_{12-24}$ at Different pHs—Since the CD spectra of $A\beta_{12-24}$ with method R showed a clear two-state conformational transition from random coil to β-sheet at pH 2.1–3.7, the thermostability of the β-structure at pH 2.2, 3.0, 3.3, 3.6, and 5.2 was measured in the temperature range of 4 to 90°C by means of θ_{214}, which is a good criterion for the peptide β-structure (Fig. 4).

The observed temperature dependence of θ_{214} at pH 2.2 was small within the overall temperature range (–2,600 ± 100 deg cm^2 $dmol^{-1}$). Because the CD spectrum at pH 2.2 and room temperature indicated the random coil conformation, this result is reasonable. The β-conformational content of the thermostable moiety over the pH range of 3.0–3.6 can be estimated by comparison with the θ_{214} intensity at 90°C at pH 2.2. Unlike the sample at pH 2.2, gradual temperature dependence of the θ_{214} intensity was observed at pH 3.0 within the temperature range of 30–90°C. When the temperature reached 84°C, the intensity became similar to that at pH 2.2, indicating that all the β-conformational moiety at a low temperature at pH 3.0 existed as a nonthermostable form and was converted to random coil as the temperature increased.

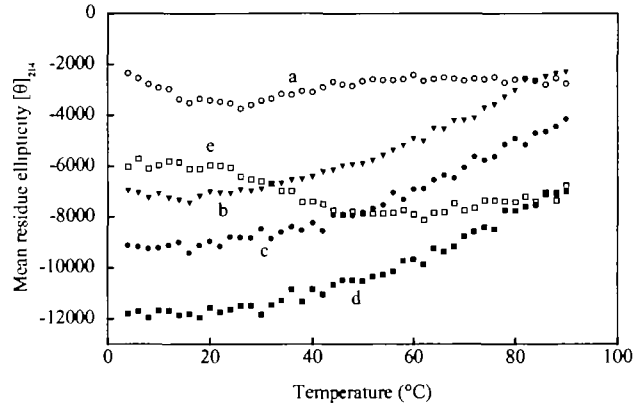

Fig. 4. **Temperature-dependent CD spectral intensity of 2 mM $A\beta_{12-24}$ at 214 nm (θ_{214}) over the pH range of 2.2–5.2.** (a) pH 2.2 (○), (b) pH 3.0 (▼), (c) pH 3.3 (●), (d) pH 3.6 (■), and (e) pH 5.2 (□). Samples were prepared by Method R. Mean residue ellipticities ($[\theta]_{214}$, degrees cm^2 $dmol^{-1}$) were plotted against temperature in the range of 4–90°C with 2°C steps.

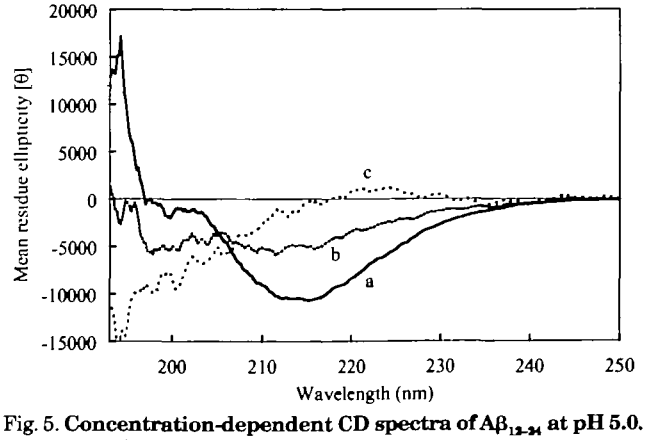

Fig. 5. **Concentration-dependent CD spectra of $A\beta_{12-24}$ at pH 5.0.** (a) 125 μM, (b) 63 μM, and (c) 31 μM.

The denatured content on conversion from the β-conformation to random coil by heating, namely the non-thermostable moiety with the β-conformation, could be estimated from the difference in θ_{214} intensity between 4 and 90°C in the plot in Fig. 4. Interestingly, these differences at pH 3.0, 3.3, and 3.6 were almost the same, values 4,700, 5,000, and 4,800 (deg cm^2 dmol^{-1}), respectively.

On the basis of these data, the existence of two types of β-conformational moieties is indicated, such as non-thermostable and thermostable ones. The amount of the non-thermostable β-conformational moiety is saturated at pH 3.0. The increase in θ_{214} intensity over all the temperature range at pH 3.3 and 3.6 compared to 3.0 suggests that thermostable aggregates with the β-conformation begin to appear between pH 3.0 and 3.3 under these sample conditions, in addition to the non-thermostable β-conformational moiety.

A small decrease in θ_{214} intensity at pH 3.0, 3.3, and 3.6 was observed on cooling from 25 to 4°C (Figs. 3A and 4). This was not surprising because such a low temperature-dependent decrease of the CD band near 217 nm for Aβ and its fragment peptide has already been reported (*31, 46, 47*).

Unlike the samples at pH 3.0, 3.3, and 3.6, the negative θ_{214} intensity of the sample at pH 5.2 gradually increased as the temperature increased from 4°C to *ca.* 40°C. Above 40°C, the intensity remained in almost the same range, –6,900 ± 1,200 deg cm^2 dmol^{-1}. This characteristic temperature dependence of the sample at pH 5.2 indicates that the aggregate exhibits strong thermostability, even at 90°C.

Concentration Dependence of CD Spectra of $A\beta_{12-24}$— Since the strong tendency towards intermolecular aggregation of $A\beta_{12-24}$ at pH 5–6 hindered conformational analysis by CD spectroscopy, the relationship between the secondary structure and peptide concentration was studied by using lower concentration peptide solutions. CD spectra of $A\beta_{12-24}$

TABLE I. **^{1}H chemical shifts and $^3J_{\alpha N}$ coupling constants of 2 mM $A\beta_{12-24}$ in water (9:1 H_2O/D_2O, 10 mM phosphate buffer) at 5°C.** (A) pH 2.2, (B) pH 3.0, (C) pH 3.3.

(A) pH 2.2

Residue	Chemical shift (ppm)[a]				$^3J_{\alpha N}$ (Hz)[b]
	NH	Hα	Hβ	Others[c]	
V12	—	3.76	2.13	γ 0.92	
H13	9.04	4.70	3.18	ε^1 8.63 δ^2 7.28	6.9
H14	8.91	4.70	3.10, 3.21	ε^1 8.63 δ^2 7.30	7.6
Q15	8.74	4.30	1.98, 2.05	γ 2.37 ε^2 7.04, 7.73	6.1
K16	8.67	4.26	1.77	γ 1.39, 1.45 δ 1.69 ε 2.99 ζ 7.62	6.0
L17	8.51	4.34	1.44, 1.60	γ 1.58 δ 0.85, 0.93	6.6
V18	8.21	4.03	1.90	γ 0.76, 0.85	8.2
F19	8.40	4.58	2.93, 2.97	$\delta^{1,2}$ 7.17 $\varepsilon^{1,2}$ 7.30	7.5
F20	8.28	4.53	2.93, 3.05	$\delta^{1,2}$ 7.22 $\varepsilon^{1,2}$ 7.32	7.5
A21	8.33	4.18	1.34		6.0
E22	8.34	4.29	1.96, 2.09	γ 2.49	6.5
D23	8.62	4.75	2.83, 2.95		7.5
V24	8.25	4.25	2.20	γ 0.94	8.0
(B) pH 3 0					
V12	—	3.76	2.13	γ 0.92	
H13	9.05	4.70	3.19	ε^1 8.63 δ^2 7.28	7.0
H14	8.92	4.70	3.11, 3.21	ε^1 8.63 δ^2 7.30	7.6
Q15	8.75	4.31	1.99, 2.05	γ 2.37 ε^2 7.05, 7.73	6.0
K16	8.67	4.26	1.77	γ 1.39, 1.45 δ 1.69 ε 2.99 ζ 7.63	5.4
L17	8.52	4.34	1.45, 1.61	γ 1.58 δ 0.86, 0.93	6.6
V18	8.20	4.03	1.91	γ 0.76, 0.85	8.7
F19	8.40	4.58	2.93, 2.98	$\delta^{1,2}$ 7.17 $\varepsilon^{1,2}$ 7.29	7.6
F20	8.29	4.53	2.93, 3.05	$\delta^{1,2}$ 7.22 $\varepsilon^{1,2}$ 7.32	7.6
A21	8.33	4.18	1.35		6.3
E22	8.34	4.30	1.96, 2.10	γ 2.49	6.5
D23	8.62	4.74	2.82, 2.94		7.5
V24	8.19	4.22	2.18	γ 0.93	8.4
(C) pH 3.3					
V12	—	3.77	2.13	γ 0.93	
H13	9.05	4.70	3.19	ε^1 8.63 δ^2 7.29	
H14	8.92	4.70	3.11, 3.21	ε^1 8.63 δ^2 7.31	
Q15	8.75	4.31	1.99, 2.05	γ 2.37 ε^2 7.05, 7.73	
K16	8.67	4.26	1.78	γ 1.38, 1.46 δ 1.69 ε 2.99 ζ 7.63	
L17	8.52	4.34	1.59	δ 0.86, 0.94	
V18	8.19	4.04	1.92	γ 0.76, 0.85	
F19	8.40	4.57	2.93, 2.99	$\delta^{1,2}$ 7.17 $\varepsilon^{1,2}$ 7.29	
F20	8.28	4.54	2.93, 3.06	$\delta^{1,2}$ 7.23 $\varepsilon^{1,2}$ 7.31	
A21	8.33	4.19	1.35		
E22	8.35	4.31	1.95, 2.10	γ 2.48	
D23	8.61	4.74	2.80, 2.93		
V24	8.08	4.18	2.16	γ 0.91	

[a]Chemical shifts in ppm were referenced to the methyl resonance of sodium 3-(trimethylsilyl)-propane sulfonate in a capillary tube. [b]Coupling constants were read from 1D or 2D E-COSY spectra. Because of signal broadening, coupling constants at pH 3.3 were not read. [c]It was not possible to distinguish the H^γ signal for L17 at pH 3.3. The H^ε signals of F19 and F20 were not assigned due to the spectral overlap.

solutions with concentrations of 31–125 μM at pH 5.0 are shown in Fig. 5. At 125 μM, the spectrum shows a negative band near 214 nm, a feature of the β-conformation. At 31 μM, however, the spectrum shows a negative band near 195 nm and a maximum band near 220 nm, clearly indicating the random coil conformation with 31 μM $A\beta_{12-24}$. The CD spectrum with 63 μM was intermediate between those with 125 and 31 μM. These spectra have an isodichroic point at 206 nm, evidence of the simple two-state β-sheet ← → random coil equilibrium described earlier.

NMR Spectra of $A\beta_{12-24}$—Although the CD results for the method R sample indicated a random coil → β-conformational transition at pH 2.1– 3.7, it was not possible to detect local conformational features for individual amino acid residues of $A\beta_{12-24}$ by CD spectroscopy. So NMR spectra were measured using 2 mM samples of $A\beta_{12-24}$ at pH 2.2, 3.0, and 3.3 with method R. A spectrum at pH 3.0 with method F was also measured, comparing the early conditions of peptide aggregation between methods R and F. All measurements were performed at 5°C, because for Aβ and its truncated peptides, a low temperature stabilizes the conformation and delays oligomerization and/or aggregation (*48*).

The high water solubility of $A\beta_{12-24}$ at acidic pH enabled even carbon NMR signals to be analyzed. This is, to our knowledge, the first report of ^{13}C chemical shift analysis of the Aβ-fragment peptide by solution NMR measurement. The ^1H chemical shifts and $^3J_{\alpha N}$ of $A\beta_{12-24}$ with method R at three pHs are summarized in Table I. Almost all the ^1H and ^{13}C NMR chemical shifts of $A\beta_{12-24}$ did not change with a pH change from 2.2 to 3.0, despite the distinct random coil to β-conformational changes detected in CD spectra. These NMR results may be explained by that the ^1H and ^{13}C chemical shifts of relatively shorter $A\beta_{12-24}$ are not so much different between the random coil and β-conformation forms, and that the differences are averaged on the NMR time scale.

Spin-Spin Coupling Constants—$^3J_{\alpha N}$ coupling constants were obtained by analysis of 1D spectra or 2D E-COSY spectra at both pH 2.2 and 3.0. The $^3J_{\alpha N}$ values are presented in Table I.

The deviations of $^3J_{\alpha N}$ coupling constants from random coil values (*49*) (ΔJ) were calculated for pH 2.2 and 3.0 (Fig. 6a). A positive ΔJ reflects the existence of the β-conformation in the peptide and protein. From V18 to the C-terminal V24 in $A\beta_{12-24}$, successive positive ΔJ values were observed at both pH 2.2 and 3.0, indicating that the region from V18 to V24 involves the β-conformation as a secondary structure at both pH 2.2 and pH 3.0 (Fig. 6a). Comparing ΔJ at pH 2.2 with that at 3.0, it can be seen that the β-conformation population at pH 3.0 increases more in the C-terminal region than that at pH 2.2. The $^3J_{\alpha N}$ analysis results thus agree with the results of CD experiments at the pH given.

$^3J_{\alpha\beta}$ coupling constants were obtained by analysis of 2D E-COSY spectra at pH 2.1 and 2.9 with a sample in 100% D_2O. The $^3J_{\alpha\beta}$ coupling constants for V12, V18, F20, D23, and V24 at both pH 2.1 and 2.9, and for F19 at pH 2.1 were

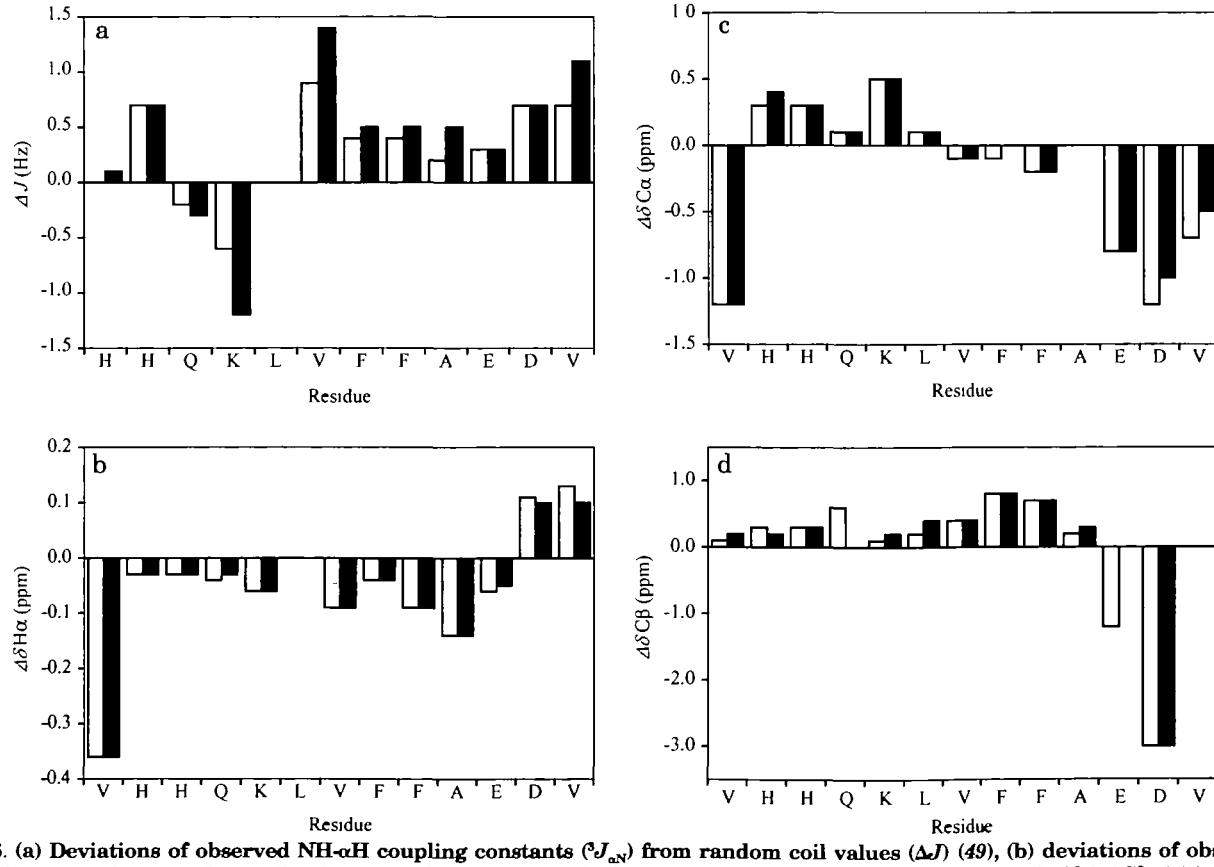

Fig. 6. **(a) Deviations of observed NH-αH coupling constants ($^3J_{\alpha N}$) from random coil values (ΔJ) (*49*), (b) deviations of observed chemical shifts from random coil values (*51*) of H^α ($\Delta\delta H^\alpha$), (c) deviations of δC^α ($\Delta\delta C^\alpha$), and (d) deviations of δC^β ($\Delta\delta C^\beta$).** (□) indicates pH 2.2 for proton in (a) and (b), and pH 2.1 for carbon in (c) and (d). (■) indicates pH 3.0 for proton in (a) and (b), and pH 2.9 for carbon in (c) and (d). The C^β signals of Q15 and E22 at pH 2.9 were not assigned due to signal broadening.

all within 5.9 and 8.3 Hz. These couplings suggest that the side chains in these residues are considerably flexible, because the values were intermediate between those for 2.6–5.1 Hz and 11.8–14.0 Hz in the well-defined staggered conformation (*50*).

Chemical Shift Deviations from the H^{α} Random Coil Value—The correlation between the chemical shift deviation from random coil reference values ($\Delta\delta$), and the type of secondary structure in proteins and peptides is well known (*51*). H^{α} conformational shifts, which are upfield in helices and downfield in β-sheets, were used to detect and analyze the secondary structure. The H^{α} chemical shifts of $A\beta_{12-24}$ at pH 2.2 and 3.0 at 5°C were compared with reference random coil values (*51*) ($\Delta\delta H^{\alpha}$) (Fig. 6b). The patterns for the two pH samples were similar, and no distinct β-conformational region was detected, although some positive deviations were observed in C-terminal D23 and V24 on NMR analysis of $\Delta\delta H^{\alpha}$.

Chemical Shifts Deviations from $^{13}C\alpha$ and $^{13}C\beta$ Random Coil Values—In $^{13}C\alpha$ and $^{13}C\beta$ chemical shifts of $A\beta_{12-24}$ at pH 2.1 and 2.9 (Table II), the chemical shifts differences in C^{α} and C^{β} between the pH 2.1 and 2.9 samples were small, *i.e.* within ± 0.2 ppm. The deviations in the chemical shifts of $^{13}C\alpha$ and $^{13}C\beta$ from random coil values (*51*) ($\Delta\delta C^{\alpha}$ and $\Delta\delta C^{\beta}$) are shown in Fig. 6c and 6d. C^{α} resonances shift downfield when located in helices and upfield when located in β-strands (*52, 53*). C^{β} resonances shift downfield when located in β-strands (*54*).

TABLE II. **^{13}C chemical shifts of 2 mM $A\beta_{12-24}$ in D_2O (10 mM phosphate buffer) at 5°C.** (A) pH 2.1, (B) pH 2.9.

(A) pH 2.1

Residue	Chemical shift (ppm)[a] Cα	Cβ[b]	Others[b]
V12	61.0	33.0	γ 20.1
H13	55.3	29.3	δ2 120.2 ε1 136.5
H14	55.3	29.3	δ2 120.3 ε1 136.5
Q15	55.8	30.0	γ 33.6
K16	56.7	33.2	γ 25.0 δ 29.4 ε 42.0
L17	55.2	42.6	γ 27.2 δ 23.7, 25.0
V18	62.1	33.3	γ 21.4, 20.8
F19	57.6	40.4	δ 132.0 ε 130.1
F20	57.5	40.3	δ 132.1 ε 131.6
A21	52.5	19.3	
E22	55.8	28.7	γ 32.7
D23	53.0	38.1	
V24	61.5	32.9	γ 21.3
(B) pH 2 9			
V12	61.0	33.1	γ 20.2
H13	55.4	29.2	δ2 120.2 ε1 136.5
H14	55.3	29.3	δ2 120.4 ε1 136.5
Q15	55.8	—	γ 33.7
K16	56.7	33.3	δ 29.4 ε 42.0
L17	55.2	42.8	δ 23.7, 25.0
V18	62.1	33.3	γ 21.4, 20.8
F19	57.7	40.4	δ 132.0 ε 130.1
F20	57.5	40.3	δ 132.1 ε 131.6
A21	52.5	19.4	
E22	55.8	—	γ 32.8
D23	53.2	38.1	
V24	61.7	32.9	γ 21.4

[a]Chemical shifts in ppm were referenced to the methyl carbon resonance of sodium 3-(trimethylsilyl)-propane sulfonate in a capillary tube. [b]It was not possible to detect the C^{β} signals for Q15 and E22, and the C^{γ} signals for K16 and L17 at pH 2.9 due to the signal broadening. The C^{γ} signals of F19 and F20 at both pH 2.1 and 2.9 were not assigned due to the spectral overlap.

C^{α} chemical shift analysis of $A\beta_{12-24}$ indicated a clear β-conformation in the C-terminal region (Fig. 6c), however, C^{β} chemical shifts did not show an obvious β-conformation in the C-terminal region (Fig. 6d). Differences on NMR analysis of $\Delta\delta C^{\alpha}$ and $\Delta\delta C^{\beta}$ may reflect the conformational features of the main and side chains of the peptide.

Since the F19–F20 moiety in Aβ is known to comprise the most important residues in the hydrophobic core (K16–A21), it is worth noting that $\Delta\delta C^{\beta}$ in F19 and F20 exceeds 0.7 ppm in Fig. 6d, indicating a distinct β-conformation at both pH 2.1 and 2.9. pH-independent β-conformational shifts indicate an important role for the intermolecular interaction in aromatic side chains of F19 and F20 of $A\beta_{12-24}$.

$\Delta\delta C^{\beta}$ of D23 showed an abnormal high field shift (Fig. 6d), and $\Delta\delta H^{\beta}$ of D23 a considerably low field shift. These findings may reflect that the side chain of D23 is situated in an unusual magnetic environment such as deshielding by the proximal phenyl group of F19 or F20.

pH-Dependence of 1D NMR Spectra—To well understand the local structures of amino acid residues in $A\beta_{12-24}$, we obtained 1D NMR spectra at pH 2.2, 3.0, and 3.3.

^1H NMR spectra in the regions of aromatic and amide protons of $A\beta_{12-24}$ are shown in Figs. 7 and 8.

Spectra in the regions of aromatic and amide protons showed broader resonances with increasing pH, which can be explained by considering either intermediate chemical exchange between isomers on the NMR time scale and/or relatively larger NMR observable aggregate sizes, and hence slower dynamics and shorter T_2.

At pH 2.2, each aromatic proton with method R showed a very sharp signal (Fig. 7d). However, at pH 3.0, line broadening was observed as a whole (Fig. 7c), especially for two aromatic protons of F19 $H^{\delta1,2}$ and F20 $H^{\delta1,2}$ (arrows), which showed larger line broadening than the sharp aromatic signals of H13 $H^{\delta2}$ and H14 $H^{\delta2}$ (arrowheads). This indicates clearly that phenyl groups of F19 and F20 are involved in special slower molecular motions.

At pH 3.3, line broadening for these aromatic signals of two phenylalanines became very large (Fig. 7a). Similar

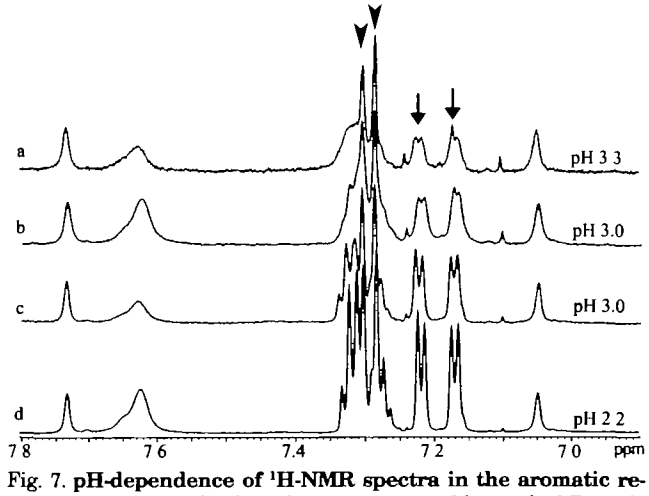

Fig. 7. **pH-dependence of ^1H-NMR spectra in the aromatic region for $A\beta_{12-24}$ at 5°C.** Samples were prepared by method R at pH 3.3 (a), 3.0 (c), and 2.2 (d). Sample b was prepared by method F at pH 3.0. The signals of F19 $H^{\delta1,2}$ and F20 $H^{\delta1,2}$ are indicated by arrows, and those of H13 $H^{\delta2}$ and H14 $H^{\delta2}$ by arrowheads.

line broadening and loss of signal intensity were found for K16 Hζ with the increase in pH (*ca.* 7.63 ppm). The N-terminal aromatic signals (H13 and H14) and amino signals of Q15 Hε2 (*ca* 7.05 and 7.73 ppm) showed little loss of signal intensity.

In Fig. 8, asterisks indicate V24 NH signals. The chemical shifts of V24 NH were markedly influenced by pH. At pH 2.2, all NH signals were relatively sharp, and the signals of H13 and V24 were much sharper, indicating faster motions in the N- and C-terminals of the peptide. Compared to the chemical shifts at pH 2.2 and 3.0, excluding the V24 NH shift, not so great changes in the chemical shifts of NH signals were observed.

Under acidic conditions at such below pH 3.0, $A\beta_{12-24}$ has overall four positive charges mainly on N-terminals, the N-terminal amino group (V12), imidazole rings of H13 and H14, and ε-amino group of K16. Electrostatic repulsion caused by N-terminal positive charges would prevent intermolecular interactions inducing self-aggregation, and thus maintain high molecular motion.

When the pH exceeds 3.0, deprotonation begins at the C-terminal carboxylate group (pK_a ca. 3.5, as determined in NMR pH titration experiments; data not shown), and hydrophobic interaction begins to surpass the weakened electrostatic repulsion. $A\beta_{12-24}$ thus mutually interacts, mainly between phenyl groups of F19 and F20. The special broadening of proton signals of F19 and F20 described above is explained by the slow aggregate motion.

At pH 3.3, considerable line broadening of NH signals was observed (Fig. 8a). The NH signals of the N-terminal region (H13 HN = 9.05 ppm, and H14 HN = 8.92 ppm), however, remained relatively sharper than those of other amino acid residues, for which J coupling constants could be read. This indicates that the N-terminal region with four positive charges exhibits higher mobility than other parts of the amino acid sequence of $A\beta_{12-24}$.

The NH signal of C-terminal V24 began to broaden between pH 3.0 and 3.3, indicating that the mobility of the C-terminal region decreased at this pH. This can be well explained by the temperature-dependence observed in CD spectra, which indicated that thermostable aggregates occurred between pH 3.0 and 3.3. Since deprotonation at the C-terminal-carboxyl group reduces the positive charge of molecules and electrostatic intermolecular repulsion among peptide molecules, it is reasonable to consider that the occurrence of the thermostable aggregates strongly correlates with the degree of deprotonation in the C-terminal carboxyl group.

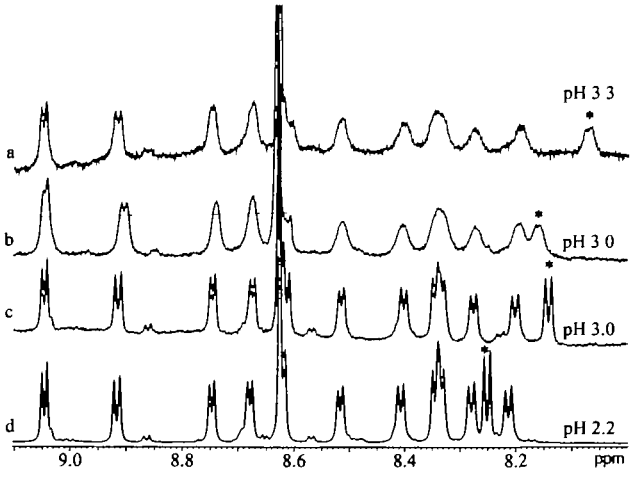

Fig. 8. **pH-dependence of ^{1}H-NMR spectra in the NH region for $A\beta_{12-24}$ at 5°C.** Samples were prepared by method R at pH 3.3 (a), 3.0 (c), and 2.2 (d). Sample b was prepared by method F at pH 3.0. The NH signals of V24 are indicated by asterisks.

On comparison of the NMR spectra obtained with methods R and F (Figs. 7, b and c, and 8, b and c), stronger signal broadening was observed with method F, despite the same pH, 3.0. This suggests that polymerization, which restricts molecular motion, in the method F sample, exceeds that with method R. The chemical shifts of the method F sample also depend on pH, and no distinct difference was seen in the chemical shifts between the samples with the two methods at the same pH.

DISCUSSION

Structural Analysis at Atomic Resolution in the Early Stage of Aggregation of $A\beta_{12-24}$—Recently, several studies suggested that not only amyloid fibrils but also soluble Aβ assemblies are neurotoxic (*4, 28*). However, there is an intrinsic difficulty in the study of the early stage of aggregation due to its scarcity and instability. Unlike full-length Aβ, $A\beta_{12-24}$ exhibits high solubility and stability even under the β-conformational conditions at pH 3.0. To study the early stages of β-amyloid peptide aggregation, we focused on the sample conditions of 2 mM $A\beta_{12-24}$ near pH 3.0. In general for Aβ and Aβ-fragment peptides, a low pH stabilizes the peptide conformation and prevents aggregation due to electrostatic effects. Fibrillation of full-length Aβ reportedly occurred, for example, at pH 4–7 (*55, 56*). For a truncated peptide such as $A\beta_{12-28}$, the acidic borderline of aggregation at 0.9 mM concentration is *ca.* pH 5.0 (*47*). The large difference in the borderline conditions for $A\beta_{12-24}$ and $A\beta_{12-28}$ is attributable to three polar residues, S-N-K, at positions 26–28 in $A\beta_{12-28}$. In addition, $A\beta_{25-28}$ is known to be the most flexible region in full-length Aβ (*57*), so for $A\beta_{12-24}$, deletion of the flexible region of $A\beta_{12-28}$ initiates aggregation under more acidic conditions.

Under the borderline conditions for aggregation of $A\beta_{12-28}$, it has been reported that a temperature-dependent random coil ⟷ β-sheet transition occurred (*47*). In our study on $A\beta_{12-24}$, we showed a pH-induced conformational transition from random coil to β-conformation at pH 2.1–3.0 by means of CD spectra. Under these conditions, NMR coupling constant ($^3J_{\alpha N}$) analysis of $A\beta_{12-24}$ showed in more detail the pH-dependent conformational transition from random coil to β-conformation in the region of V18–V24 with increasing pH (Fig. 6a). NMR chemical shift analysis of H^α and C^α of $A\beta_{12-24}$, however, yielded less information on the pH-dependent conformational transition between pH 2.2 and 3.0. Such differences in interpretation of secondary structure analysis results regarding chemical shifts and coupling constants may reflect the shortage of interstrand interaction of $A\beta_{12-24}$. A similar discussion arose on the study of the β-hairpin 16-mer and the counterpart 8-mer, where Maynard *et al.* reported that despite the β-conformation, $\Delta\delta H^\alpha$ of the 8-mer did not reflect the β-conformation such as $\Delta^3J_{\alpha N}$, and they concluded that changes in H^α chemical shift are mainly due to interstrand interactions (*58*).

As stated, chemical shift analysis of H^α and C^α for $A\beta_{12-24}$

showed a β-conformational feature in the C-terminal region, but other results of C^{β} chemical shift analysis indicated a β-conformational feature in central hydrophobic residues of F19 and F20. In the central hydrophobic region of Aβ, F19, and F20 are the residues most important for fibril formation with a hydrophobic interaction (*10, 22, 59*). In our NMR study also, the deviations from random coil values in C^{β} chemical shifts (Fig. 6d), and the beginning of marked broadening in aromatic proton signals of F19 and F20 at pH 3.0–3.3 (Fig. 7) indicated the importance of the hydrophobic interaction with these phenyl groups in early stages of the peptide assembly.

Both pH- and concentration-dependent CD spectra of $A\beta_{12-24}$ show random coil-β-conformation equilibrium (Figs. 3A and 5). Similar concentration dependence was reported for the neurotoxic Aβ-fragment peptide of $A\beta_{25-35}$ (*31*). Since β-structure formation depending on the peptide concentration was attributed to intermolecular interaction, these data strongly indicate that the intermolecular hydrophobic interaction plays a critical role in amyloid fibril formation of Aβ.

On analysis of pH-dependent NMR spectra, it became clear that the balance of the hydrophobic interaction and electrostatic repulsion determines the high order structure of $A\beta_{12-24}$. Near pH 3.0, this balance should be very sensitive to pH, because the lowest pK_a for the peptide (*ca.* 3.5 of the C-terminal carboxyl group) is close to the solution pH, and the degree of intermolecular electrostatic repulsion changes considerably with pH. pH-dependent conformational transients in the C-terminal region were also indicated on ΔJ analysis (Fig. 6a). The importance of deprotonation in the conformational transition has also been reported for full-length Aβ (*60*). Deprotonation of E22 and D23 facilitates unwinding of the helix of $A\beta_{1-40}$ in a 100 mM SDS/H_2O solution. In our experiments, deprotonation of the C-terminal carboxylate group in $A\beta_{12-24}$ corresponded to deprotonation of E22 and D23 in $A\beta_{1-40}$, because pK_a of the C-terminal carboxylate group in $A\beta_{12-24}$ is lower than that of the carboxylate groups of E22 and D23 in $A\beta_{1-40}$.

pH-Dependent Aggregation Pathway—To obtain a better understanding of the mechanism of Aβ assembly, recent attention has been focused on borderline conditions for Aβ aggregation. On the basis of the nucleation-dependent polymerization pathway (*61, 62*), this condition is called "the critical concentration for micelle formation" (*25, 26, 61*). Explanation by the nucleation-dependent mechanism well accounts for the pH dependence observed in this study with 2 mM $A\beta_{12-24}$.

Our CD results showed that almost all the $A\beta_{12-24}$ peptide in solution at pH 2.1 exists as random coil. This pH condition is well explained by the nucleation-dependent model, in which the critical concentration of micelles (c^*) at pH 2.1 exceeds 2 mM. At pH 2.1–2.7, c^* of $A\beta_{12-24}$ decreased below 2 mM and micelles began to occur. In other words, the pH range of 2.1–2.7 would be "the critical pH of micelles" for 2 mM $A\beta_{12-24}$. Taking the NMR results into account, the micelles have a β-conformation and are mainly stabilized by hydrophobic core residues including F19 and F20. The proportion of micelles in the sample solution increases as a function of pH below 3.0, being saturated at pH 3.0. At pH 3.0–3.3, the intermolecular hydrophobic interaction surpasses the intermolecular electrostatic repulsion because deprotonation of the C-terminal carboxylate group reduces the positive charge of the molecule and aggregate formation begins irreversibly. Thus, pH 3.0–3.3 of 2 mM $A\beta_{12-24}$ is considered to correspond to the critical pH of thermostable aggregates.

This pH-dependent nucleation model may explain the different aggregate forms in samples for methods R and F under the same pH conditions as follows: The greater NMR signal broadening for method F than method R at the same pH, 3.0 (Figs. 7, b and c, and 8, b and c), indicates stronger aggregate formation for method F. Increasing the pH for method F near 2.2, *i.e.* strong acidic conditions, causes the structural conversion from random coil to β-structure. This β-structural component may play a role in the seeding of nucleation of fibrils without the formation of micelles, and accumulate the irreversible aggregate formation causing the larger NMR signal broadening.

β-Structure with a Negative Shorter Wavelength Band in CD Spectra—In general, CD spectra of β-sheet in peptides and proteins, including Aβ and its fragment peptides, are characterized by a broad negative band at 217 nm and a positive band near 195 nm (*6, 31, 63, 64*). Interestingly, for our $A\beta_{12-24}$, CD spectra of β-sheet conformation showed a relatively sharp negative minimum band near 214 nm. Such non-typical β-structural CD spectra had previously been reported for Aβ and its fragment peptides. Freshly isolated protofibrils of $A\beta_{1-40}$ showed a relatively sharp negative minimum near 215 nm (*29*), and C-terminal PEG-derivatized $A\beta_{10-35}$, which forms an oligomeric β-aggregate, gave CD spectra of β-conformation with a minimum band near 215 nm (*65*). Since these CD spectra of β-conformation characterized by a relatively sharp negative minimum near 214 nm were found beyond the peptide sequence, these CD spectra are conceivably reflected by the intrinsic secondary structure, which differs from the typical β-structure in peptides.

Formation of Ribbons and Fibrils in $A\beta_{12-24}$—In studies on Aβ and its fragment peptides, in addition to amyloid fibrils, wider ribbon-like aggregates were observed (*8, 9*). Such ribbon-like aggregates of 20–30 nm in width are wider than fibrils (8–10 nm).

Such diverse aggregate morphology has been attributed to a difference in the pH of the sample solution (*9, 56, 66–68*) or the peptide sequence (*9, 19, 23, 66*). $A\beta_{9-28}$ forms amyloid-like fibrils at pH 6 and ribbons at pH 9 (*9*). Diverse polymer morphology was observed with substitutions and deletions in $A\beta_{14-23}$ (*23*). Lashuel *et al.* reported a peptidomimetic compound that forms filaments at pH 4.8 and ribbons at pH 5.7 (*68*).

Unlike the results in these reports, we have proven that $A\beta_{12-24}$ forms both fibrils and ribbons at the same pH with different preparation methods, R and F. Because the only difference between these methods is the sample dissolution protocol, variations in aggregate morphology are ascribable to the method of sample dissolution.

The solution pH immediately after sample dissolution for method R (pH 3.0) corresponds to the saturation point of micelles with β-conformation, but the conformation of the peptide with method F (pH 2.2) is random coil. This difference provides a rationale for the difference in aggregate structure despite the pH being the same. Considering that the diameter of $A\beta_{1-40}$ micelles (14 nm) is greater than the width of fibrils of 8 nm (*25*), the micelles probably act nuclei for ribbon-like aggregates (*ca.* 19 nm in width) of

$A\beta_{12-24}$ rather than fibrils (*ca.* 10 nm).

As far as we know, the longest fragment peptide of Aβ that forms ribbon-like aggregates is $A\beta_{9-28}$ (20 residues), and no ribbon-like aggregate of full-length Aβ has been reported. This indicates that, unlike fibrils, ribbon-like aggregates appear to be constructed only from shorter peptides. For this reason, it may be considered that for the Aβ fragment peptide, micelles with more than 20 residues are too unstable to form a nucleus for aggregate formation.

As described in the above discussions, the present work proved that subtle differences in the solution conditions in the early stage of aggregation of $A\beta_{12-24}$ determine whether the aggregates are fibrils or ribbons. The equilibrium between random coil and β-conformation in the solution at the early stage of aggregation is a very important factor in the process of nucleation, which causes $A\beta_{12-24}$ to grow into more highly polymerized fibrils or ribbons. The conformational equilibrium was observed not only with 2 mM $A\beta_{12-24}$ over the pH range of 2.2–3.7, but also in the concentration range below 125 μM at the near physiological pH of 5.0. The results indicate that the equilibrium exists in different solution conditions as to pH and concentration. Since it is supposed that Aβ is generated in endosomes or other low pH organelles (*69*), further study of aggregate morphology by EM and CD spectroscopy like that described in this paper may be applicable to characterization of the early stage of aggregation under more physiological conditions than those of our experimental model system.

REFERENCES

1. Pike, C.J., Burdick, D., Walencewicz, A.J., Glabe, C.G., and Cotman, C.W. (1993) Neurodegeneration induced by β-amyloid peptides in vitro: The role of peptide assembly state. *J. Neurosci.* **13**, 1676–1687
2. Seubert, P., Vigo-Pelfrey, C., Esch, F., Lee, M., Dovey, H., Davis, D., Sinha, S., Schlossmacher, M., Whaley, J., Swindlehurst, C., McCormack, R., Wolfert, R., Selkoe, D., Lieberburg, I., and Schenk, D. (1992) Isolation and quantification of soluble Alzheimer's β-peptide from biological fluids. *Nature* **359**, 325–327
3. Lorenzo, A. and Yankner, B.A. (1994) β-Amyloid neurotoxicity requires fibril formation and is inhibited by congo red. *Proc. Natl. Acad. Sci. USA* **91**, 12243–12247
4. Klein, W.L., Krafft, G.A., and Finch, C.E. (2001) Targeting small Aβ oligomers: the solution to an Alzheimer's disease conundrum? *Trends Neurosci.* **24**, 219–224
5. Teplow, D.B. (1998) Structural and kinetic features of amyloid β-protein fibrillogenesis. *Amyloid Int. J. Exp. Clin. Invest.* **5**, 121–142
6. Barrow, C.J. and Zagorski, M.G. (1991) Solution structures of β peptide and its constituent fragments: Relation to amyloid deposition. *Science* **253**, 179–182
7. Zagorski, M.G. and Barrow, C.J. (1992) NMR studies of amyloid β-peptides: Proton assignments, secondary structure, and mechanism of an α-helix → β-sheet conversion for a homologous, 28-residue, N-terminal fragment. *Biochemistry* **31**, 5621–5631
8. Gorevic, P.D., Castano, E.M., Sarma, R., and Frangione, B. (1987) Ten to fourteen residue peptides of Alzheimer's disease protein are sufficient for amyloid fibril formation and its characteristic Xray diffraction pattern. *Biochem. Biophys. Res. Commun.* **147**, 854–862
9. Fraser, P.E., Nguyen, J.T., Surewicz, W.K., and Kirschner, D.A. (1991) pH-dependent structural transitions of Alzheimer amyloid peptides. *Biophys. J.* **60**, 1190–1201
10. Esler, W.P., Stimson, E.R., Ghilardi, J.R., Lu, Y.A., Felix, A.M., Vinters, H.V., Mantyh, P.W., Lee, J.P., and Maggio, J.E. (1996) Point substitution in the central hydrophobic cluster of a human β-amyloid congener disrupts peptide folding and abolishes plaque competence. *Biochemistry* **35**, 13914–13921
11. Soto, C., Sigurdsson, E.M., Morelli, L., Kumar, R.A., Castaño, E.M., and Frangione, B. (1998) β-Sheet breaker peptides inhibit fibrillogenesis in a rat brain model of amyloidosis: Implications for Alzheimer's therapy. *Nat. Med.* **4**, 822–826
12. Talafous, J., Marcinowski, K.J., Klopman, G., and Zagorski, M.G. (1994) Solution structure of residue 1–28 of the amyloid β-peptide. *Biochemistry* **33**, 7788–7796
13. Lee, J.P., Stimson, E.R., Ghilardi, J.R., Mantyh, P.W., Lu, Y.-A., Felix, A.M., Llanos, W., Behbin, A., Cummings, M., Van Criekinge, M., Timms, W., and Maggio, J.E. (1995) 1H NMR of Aβ amyloid peptide congeners in water solution. Conformational changes correlate with plaque competence. *Biochemistry* **34**, 5191–5200
14. Jayawickrama, D., Zink, S., Vander Velde, D., Effiong, R.I., and Larive, C.K. (1995) Conformational analysis of the β-amyloid peptide fragment, β(12–28). *J. Biomol. Struct. Dyn.* **13**, 229–244
15. Kohno, T., Kobayashi, K., Maeda, T., Sato, K., and Takashima, A. (1996) Three-dimensional structures of the amyloid β-peptide (25–35) in membrane-mimicking environment. *Biochemistry* **35**, 16094–16104
16. Nguyen, J., Baldwin, M.A., Cohen, F.E., and Prusiner, S.B. (1995) Prion protein peptides induce α-helix to β-sheet conformational transitions. *Biochemistry* **34**, 4186–4192
17. Ragg, E., Tagliavini, F., Malesani, P., Monticelli, L., Bugiani, O., Forloni, G., and Salmona, M. (1999) Determination of solution conformations of PrP106–126, a neurotoxic fragment of prion protein by ^{1}H NMR and restrained molecular dynamics. *Eur. J. Biochem.* **266**, 1192–1201
18. MacPhee, C.E. and Dobson, C.M. (2000) Chemical dissection and reassembly of amyloid fibrils formed by a peptide fragment of transthyretin. *J. Mol. Biol.* **297**, 1203–1215
19. Hilbich, C., Kisters-Woike, B., Reed, J., Masters, C.L., and Beyreuther, K. (1992) Substitutions of hydrophobic amino acids reduce the amyloidogenicity of Alzheimer's disease βA4 peptides. *J. Mol. Biol.* **228**, 460–473
20. Tjernberg, L.O., Näslund, J., Lindqvist, F., Johansson, J., Karlström, A.R., Thyberg, J., Terenius, L., and Nordstedt, C. (1996) Arrest of β-amyloid fibril formation by a pentapeptide ligand. *J. Biol. Chem.* **271**, 8545–8548
21. Tjernberg, L.O., Lilliehöök, C., Callaway, D.J.E., Näslund, J., Hahne, S., Thyberg, J., Terenius, L., and Nordstedt, C. (1997) Controlling amyloid β-peptide fibril formation with protease-stable ligands. *J. Biol. Chem.* **272**, 12601–12605
22. Mansfield, S.L., Jayawickrama, D.A., Timmons, J.S., and Larive, C.K. (1998) Measurement of peptide aggregation with pulsed-field gradient nuclear magnetic resonance spectroscopy. *Biochim. Biophys. Acta* **1382**, 257–265
23. Tjernberg, L.O., Callaway, D.J.E., Tjernberg, A., Hahne, S., Lilliehöök, C., Terenius, L., Thyberg, J., and Nordstedt, C. (1999) A molecular model of Alzheimer amyloid β-peptide fibril formation. *J. Biol. Chem.* **274**, 12619–12625
24. Balbach, J.J., Ishii, Y., Antzutkin, O.N., Leapman, R.D., Rizzo, N.W., Dyda, F., Reed, J., and Tycko, R. (2000) Amyloid fibril formation by Aβ16–22, a seven-residue fragment of the Alzheimer's β-amyloid peptide, and structural characterization by solid state NMR. *Biochemistry* **39**, 13748–13759
25. Lomakin, A., Chung, D.S., Benedek, G.B., Kirschner, D.A., and Teplow, D.B. (1996) On the nucleation and growth of amyloid β-protein fibrils: Detection of nuclei and quantitation of rate constants. *Proc. Natl. Acad. Sci. USA* **93**, 1125–1129
26. Lomakin, A., Teplow, D.B., Kirschner, D.A., and Benedek, G.B. (1997) Kinetic theory of fibrillogenesis of amyloid β-protein. *Proc. Natl. Acad. Sci. USA* **94**, 7942–7947
27. Malinchik, S.B., Inouye, H., Szumowski, K.E., and Kirschner, D.A. (1998) Structural analysis of Alzheimer's β(1–40) amyloid: Protofilament assembly of tubular fibrils. *Biophys. J.* **74**, 537–545
28. El-Agnaf, O.M.A., Mahil, D.S., Patel, B.P., and Austen, B.M. (2000) Oligomerization and toxicity of β-amyloid-42 implicated in Alzheimer's disease. *Biochem. Biophys. Res. Commun.* **273**, 1003–1007
29. Walsh, D.M., Hartley, D.M., Kusumoto, Y., Fezoui, Y., Condron,

M.M., Lomakin, A., Benedek, G.B., Selkoe, D.J., and Teplow, D.B. (1999) Amyloid β-protein fibrillogenesis. *J. Biol. Chem.* **274**, 25945–25952
30. Hasegawa, K., Yamaguchi, I., Omata, S., Gejyo, D., and Naiki, H. (1999) Interaction between Aβ(1–42) and Aβ(1–40) in Alzheimer's β-amyloid fibril formation *in vitro*. *Biochemistry* **38**, 15514–15521
31. Terzi, E., Hölzemann, G., and Seelig, J. (1994) Reversible random coil-β-sheet transition of the Alzheimer β-amyloid fragment (25–35). *Biochemistry* **33**, 1345–1350
32. Piantini, U., Sørensen, O.W., and Ernst, R.R. (1982) Multiple quantum filters for elucidating NMR coupling networks. *J. Am. Chem. Soc.* **104**, 6800–6801
33. Shaka, A.J. and Freeman, R. (1983) Simplification of NMR spectra by filtration through multiple-quantum coherence. *J. Magn. Reson.* **51**, 169–173
34. Macura, S. and Ernst, R.R. (1980) Elucidation of cross-relaxation in liquids by two-dimensional NMR spectroscopy. *Mol. Phys.* **41**, 95–117
35. Bax, A. and Davis, D.G. (1985) Practical aspects of two-dimensional transverse NOE spectroscopy. *J. Magn. Reson.* **63**, 207–213
36. Delaglio, F., Grzesiek, S., Vuister, G.W., Zhu, G., Pfeifer, J., and Bax, A. (1995) NMRPipe: A multidimensional spectral processing system based on UNIX pipes. *J. Biomol. NMR* **6**, 277–293
37. Marion, D. and Wüthrich, K. (1983) Application of phase sensitive two-dimensional correlated spectroscopy (COSY) for measurements of ^{1}H-^{1}H spin-spin coupling constants in proteins. *Biochem. Biophys. Res. Commun.* **113**, 967–974
38. Piotto, M., Saudek, V., and Sklenar, V. (1992) Gradient-tailored excitation for single-quantum NMR spectroscopy of aqueous solutions. *J. Biomol. NMR* **2**, 661–665
39. Kay, L.E. (1995) Pulsed field gradient multi-dimensional NMR methods for the study of protein structure and dynamics in solution. *Prog. Biophys. Mol. Biol.* **63**, 277–299
40. Griesinger, C., Søorensen, O.W., and Ernst, R.R. (1987) Practical aspects of the E.COSY technique. Measurement of scalar spin-spin coupling constants in peptides. *J. Magn. Reson.* **75**, 474–492
41. Bax, A., Griffey, R.H., and Hawkins, B.L. (1983) Correlation of proton and nitrogen-15 chemical shifts by multiple quantum NMR. *J. Magn. Reson.* **55**, 301–315
42. Shaka, A.J., Barker, P.B., and Freeman, R. (1985) Computer-optimized decoupling scheme for wideband applications and low-level operation. *J. Magn. Reson.* **64**, 547–552
43. Wüthrich, K. (1986) *NMR of Proteins and Nucleic Acids*, Wiley, New York
44. Forman-Kay, J.D., Clore, G.M., and Gronenborn, A.M. (1992) Relationship between electrostatics and redox function in human thioredoxin: Characterization of pH titration shifts using two-dimensional homo- and heteronuclear NMR. *Biochemistry* **31**, 3442–3452
45. Nielsen, E.H., Nybo, M., and Svehag, S.E. (1999) Electron microscopy of prefibrillar structures and amyloid fibrils. *Methods Enzymol.* **309**, 491–496
46. Gursky, O. and Aleshkov, S. (2000) Temperature-dependent β-sheet formation in β-amyloid Aβ(1-40) peptide in water: uncoupling β-structure folding from aggregation. *Biochim. Biophys. Acta* **1476**, 93–102
47. Jarvet, J., Damberg, P., Bodell, K., Eriksson, L.E.G., and Gräslund, A. (2000) Reversible random coil to β-sheet transition and the early stage of aggregation of the Aβ(12–28) fragment from the Alzheimer peptide. *J. Am. Chem. Soc.* **122**, 4261–4268
48. Kusumoto, Y., Lomakin, A., Teplow, D.B., and Benedek, G.B. (1998) Temperature dependence of amyloid β-protein fibrillization. *Proc. Natl. Acad. Sci. USA* **95**, 12277–12282
49. Smith, L.J., Bolin, K.A., Schwalbe, H., MacArthur, M.W., Thornton, J.M., and Dobson, C.M. (1996) Analysis of main chain torsion angles in proteins: Prediction of NMR coupling constants for native and random coil conformations. *J. Mol. Biol.* **255**, 494–506
50. Basus, V.J. (1989) Proton nuclear magnetic resonance assignments. *Methods Enzymol.* **177**, 132–149
51. Wishart, D.S., Bigam, C.G., Holm, A., Hodges, R.S., and Sykes, B.D. (1995) ^{1}H, ^{13}C and ^{15}N random coil NMR chemical shifts of the common amino acids. I. Investigations of nearest-neighbor effects. *J. Biomol. NMR* **5**, 67–81
52. Saito, H. (1986) Conformation-dependent ^{13}C chemical shifts: A new means of conformational characterization as obtained by high-resolution solid-state ^{13}C NMR. *Magn. Reson. Chem.* **24**, 835–852
53. Wishart, D.S., Sykes, B.D., and Richards, F.M. (1991) Relationship between nuclear magnetic resonance chemical shift and protein secondary structure *J. Mol. Biol.* **222**, 311–333
54. Spera, S. and Bax, A. (1991) Empirical correlation between protein backbone conformation and Cα and Cβ ^{13}C nuclear magnetic resonance chemical shifts. *J. Am. Chem. Soc.* **113**, 5490–5492
55. Esler, W.P., Stimson, E.R., Ghilardi, J.R., Vinters, H.V., Lee, J.P., Mantyh, P.W., and Maggio, J.E. (1996) *In vitro* growth of Alzheimer's disease β-amyloid plaques displays first-order kinetics. *Biochemistry* **35**, 749–757
56. Wood, S.J., Maleeff, B., Hart, T., and Wetzel, R. (1996) Physical, morphological and functional differences between pH 5.8 and 7.4 aggregates of the Alzheimer's amyloid peptide Aβ. *J. Mol. Biol.* **256**, 870–877
57. Shao, H., Jao, S., Ma, K., and Zagorski, M.G. (1999) Solution structures of micelle-bound amyloid β-(1–40) and β-(1–42) peptides of Alzheimer's disease. *J. Mol. Biol.* **285**, 755–773
58. Maynard, A.J., Sharman, G.J., and Searle, M.S. (1998) Origin of β-hairpin stability in solution: Structural and thermodynamic analysis of the folding of a model peptide supports hydrophobic stabilization in water. *J. Am. Chem. Soc.* **120**, 1996–2007
59. Wood, S.J., Wetzel, R., Martin, J.D., and Hurle, M.R. (1995) Prolines and amyloidogenicity in fragments of the Alzheimer's peptide β/A4. *Biochemistry* **34**, 724–730
60. Coles, M., Bicknell, W., Watson, A.A., Fairlie, D.P., and Craik, D.J. (1998) Solution structure of amyloid β-peptide(1–40) in a water-micelle environment. Is the membrane-spanning domain where we think it is? *Biochemistry* **37**, 11064–11077
61. Harper, J.D. and Lansbury, P.T. (1997) Models of amyloid seeding in Alzheimer's disease and scrapie: mechanistic truths and physiological consequences of the time-dependent solubility of amyloid proteins. *Annu. Rev. Biochem.* **66**, 385–407
62. Jarrett, J.T. and Lansbury, P.T. (1993) Seeding "One-dimensional crystallization" of amyloid: A pathogenic mechanism in Alzheimer's disease and scrapie? *Cell* **73**, 1055–1058
63. Colón, W. (1999) Analysis of protein structure by solution optical spectroscopy. *Methods Enzymol.* **309**, 605–632
64. Fletcher, T.G. and Keire, D.A. (1997) The interaction of β-amyloid protein fragment (12–28) with lipid environments. *Protein Sci.* **6**, 666–675
65. Burkoth, T.S., Benzinger, T.L.S., Jones, D.N.M., Hallenga, K., Meredith, S.C., and Lynn, D.G. (1998) C-terminal PEG blocks the irreversible step in β-amyloid(10–35) fibrillogenesis. *J. Am. Chem. Soc.* **120**, 7655–7656
66. Fraser, P.E., McLachlan, D.R., Surewicz, W.K., Mizzen, C.A., Snow, A.D., Nguyen, J.T., and Kirschner, D.A. (1994) Conformation and fibrillogenesis of Alzheimer Aβ peptides with selected substitution of charged residues. *J. Mol. Biol.* **244**, 64–73
67. Huang, T.H.J., Yang, D.S., Plaskos, N.P., Go, S., Yip, C.M., Fraser, P.E., and Chakrabartty, A. (2000) Structural studies of soluble oligomers of the Alzheimer β-amyloid peptide. *J. Mol. Biol.* **297**, 73–87
68. Lashuel, H.A., LaBrenz, S.R., Woo, L., Serpell, L.C., and Kelly, J.W. (2000) Protofilaments, filaments, ribbons, and fibrils from peptidomimetic self-assembly: Implications for amyloid fibril formation and materials science. *J. Am. Chem. Soc.* **122**, 5262–5277
69. Sommer, B. (2002) Alzheimer's disease and the amyloid cascade hypothesis: ten years on. *Curr. Opin. Pharmacol.* **2**, 87–92
70. Markley, J.L., Bax, A., Arata, Y., Hilbers, C.W., Kaptein, R., Sykes, B.D., Wright, P.E., and Wüthrich, K. (1998) Recommendations for the presentation of NMR structures of proteins and nucleic acids. *Eur. J. Biochem.* **256**, 1–15